

## Article

# Crosslinked Polymer Coatings of Poly (Acrylic Acid-co-acrylamide)/Polyethyleneimine (P(AA-co-AAm)/PEI) on Titanium Alloy with Excellent Lubrication Performance for Artificial Joints

Yaling Deng <sup>1,\*</sup>, Yu Xu <sup>1,2</sup>, Lei Nie <sup>3,\*</sup>  and Yiyang Huang <sup>1</sup>

<sup>1</sup> College of Intelligent Science and Control Engineering, Jinling Institute of Technology, Nanjing 211169, China; jtxuyu@jit.edu.cn (Y.X.); 15850776085@163.com (Y.H.)

<sup>2</sup> State Key Laboratory of Organic Electronics and Information Displays, Institute of Advanced Materials (IAM), Nanjing University of Posts & Telecommunications, 9 Wenyuan Road, Nanjing 210023, China

<sup>3</sup> College of Life Sciences, Xinyang Normal University (XYNU), Xinyang 464000, China

\* Correspondence: yalingdeng@jit.edu.cn (Y.D.); nieleifu@yahoo.com or nielei@xynu.edu.cn (L.N.); Tel.: +86-13600621068 (L.N.)

**Abstract:** The development of coatings with efficient lubrication and load-bearing capacity is an urgent need for artificial joints. Here, we successfully fabricated poly (acrylic acid-co-acrylamide)/polyethyleneimine (P(AA-co-AAm)/PEI) coating on titanium alloy (Ti6Al4V) surface via UV irradiation and thermal treatment technique. The dual crosslinked network structures were composed of a P(AA-co-AAm) network via free radical polymerization and a PAA-co-PEI network via thermal crosslinking of amine and carboxyl groups. The thermally crosslinked P(AA-co-AAm)/PEI coatings exhibit a stable low friction coefficient (approximately 0.022) and exceptionally low wear volume, with a 93.8% and 92.6% reduction, respectively, in comparison to the pristine Ti6Al4V. These thermally crosslinked P(AA-co-AAm)/PEI hydrogel coatings exhibit excellent lubrication and anti-wear properties, providing a strategy for developing novel lubricating coatings in the biomedical field.

**Keywords:** thermal crosslinking; polymer coating; friction; super low wear



**Citation:** Deng, Y.; Xu, Y.; Nie, L.; Huang, Y. Crosslinked Polymer Coatings of Poly (Acrylic Acid-co-acrylamide)/Polyethyleneimine (P(AA-co-AAm)/PEI) on Titanium Alloy with Excellent Lubrication Performance for Artificial Joints. *Coatings* **2024**, *14*, 28. <https://doi.org/10.3390/coatings14010028>

Academic Editor: Csaba Balázsi

Received: 17 November 2023

Revised: 22 December 2023

Accepted: 22 December 2023

Published: 25 December 2023



**Copyright:** © 2023 by the authors. Licensee MDPI, Basel, Switzerland. This article is an open access article distributed under the terms and conditions of the Creative Commons Attribution (CC BY) license (<https://creativecommons.org/licenses/by/4.0/>).

## 1. Introduction

Natural joint systems, including bone as the backing materials, articular cartilage as the robust bearing interface, and viscous synovial fluid as the lubricant, provide an extremely low friction coefficient of less than 0.03 at the interface and the high load carrying capacity (7–9 times the weight of the human body) [1–4]. However, the motor function of natural joints is susceptible to various factors, such as the aging population, congenital diseases, osteoarthritis, and acute trauma. About 300 million people suffer from arthritis worldwide, and the age is getting younger [5]. These have a negative effect on the frictional characteristics and subsequent degeneration of the joint surface.

Artificial joint replacement is the ultimate effective treatment to restore the normal function of joint movement and ameliorate the lives of patients. A variety of materials, such as metal materials, ceramic materials, and polymer materials, are employed in artificial joints. Titanium and its alloys are the most widely used as main metal materials for joint prostheses and other implants due to their chemical stability, mechanical properties, corrosion resistance, and biocompatibility [6,7]. However, the effective life of artificial hips and knees is limited to approximately 15 years [8]. The primary factor behind the limitation of the effective long-term service of titanium alloy is the poor tribological properties of high friction coefficient and low wear resistance [9]. Furthermore, patients who obtained total joint replacement (THR) are becoming younger, along with more active and athletic [10]. As a result, strenuous activities between artificial joint materials generate more wear particles

and aggravate wear damage, leading to aseptic joint loosening and periprosthetic osteolysis [11,12]. That hinders practical development and reduces the service life. Therefore, the reduction in friction and wear between the head and cup is a main issue for improving the lifetime of the artificial joints.

Surface functionalization is a feasible and promising strategy to overcome these issues to prevent joint loosening caused by abrasive debris. Surface coating improves the physicochemical properties and functions without altering the main properties of the substrate [13,14]. For example, the polyelectrolyte multilayers prepared with layer-by-layer technology endow the desired properties, such as corrosion resistance [15], antibacterial [16], hydrophilicity [17], and excellent tribological performance [18,19]. The hydrated layer formed with grafting polymer brushes improves effective lubrication for artificial joints [20,21]. Therefore, preparing hydrophilic polymer coating on the device surface is an effective strategy. The hydrophilic polymer hydrogel has a three-dimensional porous network structure and water content similar to that of natural articular cartilage, accompanied by suitable biocompatibility and lubrication properties [22,23]. That has been widely utilized in articular cartilage repair. For example, the combination of methacrylated gelatin gum (GGMA) hydrogel and chondrocytes and adipose mesenchymal stromal/stem cells achieved expression of intense collagen type II, low collagen type I gene, and protein [24]. It also supports full-layer regeneration of critical-size lesions with suitable integration/bonding with natural cartilage after 8 weeks of treatment. Hybrid photocrosslinkable (HPC) hydrogel of methacrylate-grafted hyaluronic acid (HA) with *o*-nitrobenzyl (NB) anchored to the surrounding cartilage with a gelation rate of less than 2 s [25]. When the hydrogel was implanted in pigs for 6 months, the defects of knee joints were repaired well, and the interface showed cartilage-like tissue with satisfactory healing.

A variety of polymers, such as poly (vinyl alcohol) (PVA) [26], polyacrylamide (PAAm) [27], and polyacrylic acid (PAA) [19], have been employed for hydrogel preparation. Among these materials, polyacrylamide (PAAm), as a soft and ductile neutral poly hydrogel, is a highly expandable platform [28]. It is well known that polyacrylamide-based hydrogels have suitable biocompatibility. It does not have any toxic effects on human fibroblasts, along with the properties of non-carcinogenic, non-toxic, and non-allergenic, while providing resistance to certain enzymes and microbial degradation in the body [29,30]. However, pristine PAAm hydrogels are soft and fragile [31], which is not suitable for load-bearing applications. Its function and mechanical properties can be adjusted by adding other chemical components [32]. Adding acrylic acid (AA) to the PAAm network is a common method to strengthen PAAm hydrogels via free radical polymerization [19,33]. The high density of hydrophilic carboxyl groups induces the conformation expansion of the polymer chain [34]. Due to the greater flexibility of the polymer chain, the introduction of AA improves the equilibrium swelling ratio value and contributes to a decrease in brittleness [35]. However, high friction and non-wear resistance are usually serious issues in the hydrogel. The severe surface damage even restricts the long-term stability of hydrogels.

Polyethyleneimine (PEI), with a large number of amine groups per molecule, has several advantageous properties, such as high hydrophilicity, biocompatibility, and commercial availability. Its high molecular weight, high branched structure, and high molecular entanglement provide high elastic properties [36]. As a cationic polyelectrolyte, PEI can also strongly attract anionic molecules via a weak bonding force of electrostatic interactions, such as PAA [37]. Therefore, it has the ability to participate in the formation of a polymeric hydrogel network to improve its properties. The electrostatic interaction of cationic and anionic molecules can be transformed into a more robust covalent bond via crosslinking components with heat treatment [38]. Compared with electrostatic interaction, covalent bonding enhances the connection between polymer molecules. That increases the surface hardness and improves the bond strength of the polymer films [39].

Herein, we designed a series of P(AA-*co*-AAm)/PEI (poly(acrylic acid-*co*-acrylamide)/polyethyleneimine) composite hydrogel coatings on Ti6Al4V substrate with the expectation of suitable lubrication, load-bearing, and anti-wear perspectives. In this work, acrylic acid

and acrylic amide were selected as the hydrogel matrix monomers due to their potential to expand more functions and deserve further study. As pristine P(AA-co-AAm) hydrogel is soft and weak, and then PEI was introduced into the polymeric matrix of P(AA-co-AAm) hydrogels to form a crosslinking network to enhance the strengthening of the hydrogel matrix via thermal crosslinking. By characterizing composite hydrogel coating's tribological properties, this study will guide the design of low friction and anti-wear coating.

## 2. Experimental Section

### 2.1. Materials and Reagents

Medical-grade Ti6Al4V discs with the dimensions of 30 mm (diameter) and 5 mm (thickness) were supplied by Botai Metal Materials Co., Ltd. (Baoji, China). Acrylic acid (AA), acrylamide (AAm), polyethyleneimine (PEI, M.W. 70,000, 50%), triethylene glycol dimethacrylate (TEGDMA), and 2-hydroxy-2-methyl-propiophenone were purchased from Aladdin Reagent Co., Ltd. (Los Angeles, CA, USA). All reagents were used without further purification. Triethylene glycol dimethacrylate (TEGDMA) and 2-hydroxy-2-methyl-propiophenone were employed as the crosslinker and UV initiator. Deionized water was obtained using a water purification system with a resistivity of  $18.2 \text{ M}\Omega \cdot \text{cm}^{-1}$  and then utilized in the process of synthesis and swelling measurements.

### 2.2. Preparation of Hydrogel-Coated Ti6Al4V

Ti6Al4V discs were coarsely ground with grit sandpapers of 320, 600, 800, 1000. Then, polishing was carried out with nylon polishing cloth containing  $2.6 \mu\text{m}$  alumina suspension and  $1 \mu\text{m}$  diamond suspension to obtain similar roughness,  $R_a \approx 0.06 \mu\text{m}$  (Figure 1). The roughness was evaluated by a non-contact three-dimensional white light interferometer (Rtec Instruments, San Jose, CA, USA). All the substrates were cleaned in acetone, ethanol, and deionized water under ultrasonication for 20 min to eliminate contaminants. The rinsed discs were dipped into dopamine solution (2 mg/mL in 10 mM Tris, pH 8.5) for 24 h in the dark to obtain a polydopamine (PDA) anchoring layer. Polydopamine (PDA), as a widely used adhesive material, is used to functionalize various surfaces due to its high catechol content [40,41].

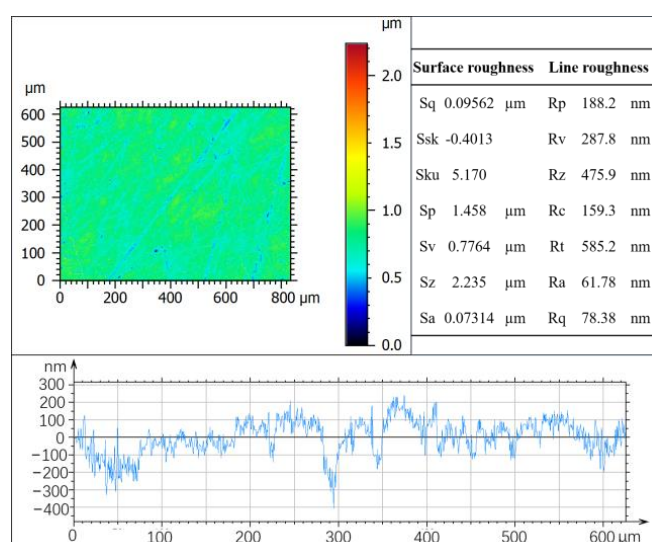


**Figure 1.** The surface roughness and line roughness of polished Ti6Al4V.

The hydrogel-coated Ti6Al4V was prepared via UV irradiation technology and thermal treatment. Firstly, TEGDMA (1.5  $v/v\%$ ), 2-hydroxy-2-methyl-propiophenone (0.4  $v/v\%$ ), AA (3 mol/L), AAm (1 mol/L), and PEI solutions with different parameters were dissolved in deionized water to form hydrogel complex solution. The volume fraction was relative to the composite solution. The PEI parameters were set relative to the weight of AA, including

5%, 7.5%, 10%, 12.5%, and 15%. The composite solution was degassed with nitrogen for 10 min to remove oxygen.

The Ti6Al4V alloy substrate pretreated with PDA was placed into a mold. The hydrogel complex solution was poured into the mold and covered with a quartz plate. The intermediate distance between the Ti6Al4V substrate and quartz plate filling with solution was controlled at 1 mm. After that, the hydrogel complex solution was polymerized to form P(AA-co-AAm)/PEI hydrogel coating under UV irradiation for 20 min. A 500 W high-pressure mercury lamp (Beijing Institute of electric light source) was utilized to initiate polymerization. The passage of ultraviolet light was limited to wavelengths of  $350 \pm 50$  nm via a polypropylene film filter. Finally, the covalent bond crosslinking process of P(AA-co-AAm)/PEI coatings was conducted by heating at  $150^\circ\text{C}$  for 1 h in a vacuum oven and then cooled to ambient temperature. The preparation procedure is depicted in Figure 2.

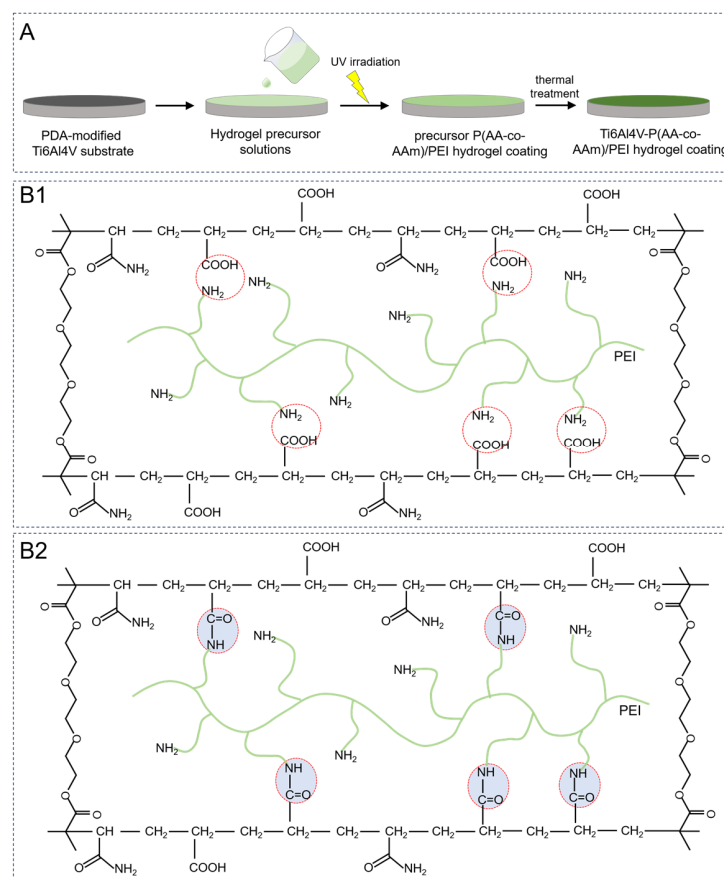


**Figure 2.** The preparation procedure (A) and schematic diagram of the structure and bonding of P(AA-co-AAm)/PEI coating before and after thermal crosslinking (B). The bond force of amine groups in PEI and carboxyl groups in PAA converted from electrostatic interaction (B1) to the covalent bond formation (B2). (The red circles are the functional groups participating in thermal crosslinking).

### 2.3. Structural Characterization

The surface chemical compositions were examined by Fourier transform infrared (FTIR, VERTEX 80 V, Bruker, Ettlingen, Germany) and X-ray photoelectron spectroscopy (XPS, Thermo Scientific K-Alpha, Waltham, MA, USA). Scanning electron microscopy (SEM, FEI Scios 2 HiVac, Hillsboro, OR, USA) was used to observe the morphology. The crystal structures of the samples were characterized by an X-ray diffractometer instrument (XRD, Bruker, D8 Advance, Ettlingen, Germany) with  $K\alpha$  radiation ( $\lambda = 0.15418$  nm).

#### 2.4. Equilibrium Water Content Measurement

The equilibrium water content was calculated from the weight of the water-equilibrated ( $W_w$ ) and dried sample ( $W_d$ ) according to the equations [42]

$$\text{Equilibrium water content (wt\%)} = \frac{W_w - W_d}{W_w} \times 100\%$$

Five samples were measured for each hydrogel to provide an average value.

#### 2.5. Porosity Measurement

According to Archimedes' principle, the porosity was calculated using the following equation [43,44]:

$$\text{Porosity (\%)} = \frac{W_2 - W_1}{W_3 - W_2} \times 100\%$$

where  $W_1$  represents the mass of the dry hydrogel,  $W_2$  is the mass of the swelling hydrogel in air, and  $W_3$  represents the mass of the swelling hydrogel suspended in deionized water. All the measurements were performed five times for each type of sample.

#### 2.6. Water Contact Angle Measurements

The water contact angle was used to estimate the hydrophilicity of P(AA-co-AAm)/PEI coatings. The measurement was carried out using a deionized water droplet by a JY-82 instrument. Five different positions of the specimen were analyzed to obtain the average value.

#### 2.7. Thermal Characterization

Thermal stability characteristics of the hydrogel coatings were evaluated using a thermal gravimetric instrument (TA-Q600, TA Instruments, New Castle, DE, USA). The data of thermogravimetry and differential scanning calorimetry (TA-Q600, TA Instruments, New Castle, DE, USA) were collected simultaneously during the same experiment. Nitrogen, as a protective gas, was utilized to prevent oxidation at high temperatures. The experimental temperatures were set from 30 to 400 °C at a heating rate of 10 °C min<sup>-1</sup>.

#### 2.8. Measurement of Tribological Properties

The friction coefficients and wear experiments were performed on a ball-on-disk tribometer (MS-T3001, Lanzhou Huahui Instrument Technology, Lanzhou, China) using a rotating sliding mode with a sliding test radius of 8 mm. Stainless balls (316 L, diameter: 6 mm) were utilized as a static counterpart. Deionized water, saline, and calf serum were employed as lubricants. The conditions are 1 N, 117 rpm, 0.1 m/s for about 50 min at room temperature. The hardness of precursor P(AA-co-AAm)/PEI hydrogel material and thermally crosslinked P(AA-co-AAm)/PEI hydrogel materials are about 4.1 HV and 15.4 HV. The Hertzian contact pressure is about 18 MPa. The wear morphology and wear volume of the ball and samples were characterized utilizing a non-contact three-dimensional white light interferometer (Rtec Instruments, San Jose, CA, USA). The wear surface of the coating was also examined by scanning electron microscopy (SEM, FEI Scios 2 HiVac) to evaluate the wear mechanism. Moreover, the experimental results were obtained by repeating three independent tests to obtain average values.

### 3. Results and Discussion

#### 3.1. Preparation of P(AA-co-AAm)/PEI Coating on Ti6Al4V

As a joint prosthesis, the lubricating and wear-resistant properties of Ti6Al4V were still limited when employed as artificial joints. Herein, inspired by the stratified structure of the natural joint lubrication system, the P(AA-co-AAm)/PEI hydrogel coating was prepared on the surface of Ti6Al4V to enhance its friction reduction and wear resistance. The preparation procedure is depicted in Figure 2A.

Firstly, precursor P(AA-co-AAm)/PEI hydrogel coating was prepared via UV-initiated polymerization. The 2-hydroxy-2-methyl-propiophenone could initiate to generate free radicals under UV irradiation. The initiator and crosslinker resulted in the polymerization of AA/AAm monomers and the formation of hydrogel coating on the substrate. The chemical bonds between the AA monomer and AAm monomer were formed (Figure 2(B1)), which fabricated the first crosslinked network structure. The electrostatic absorption interactions occurred between carboxyl groups in AA molecules and amide groups in PEI molecules. Subsequently, precursor P(AA-co-AAm)/PEI hydrogel was annealed via thermal treatment. The samples were exposed to a temperature of 150 °C and applied vacuum. The thermal crosslinking process represented a simple condensation reaction between amine groups of PEI and carboxyl groups of PAA, resulting in the formation of amide linkages and currently generating water as a byproduct (Figure 2(B2), red circle). The second crosslinked network structure was established.

### 3.2. Chemical Composition and Surface Morphology

FTIR, XRD, SEM, and XPS were conducted to characterize the structure and chemical compositions of hydrogel coating. As depicted in Figure 3a, the peaks at 796, 1166, and 1447  $\text{cm}^{-1}$  simultaneously appear in precursor P(AA-co-AAm)/PEI hydrogel and thermally treated hydrogel. The characteristic peak at 796  $\text{cm}^{-1}$  is assigned to the stretching vibration of the methylene group. The wavenumber at 1166  $\text{cm}^{-1}$  corresponds to the spectral band of  $-\text{C}-\text{N}-$  stretching [45]. The absorption peak at 1447  $\text{cm}^{-1}$  represents the  $\text{C}-\text{N}$  stretching vibration of amine in the AM and PEI [46,47]. For precursor P(AA-co-AAm)/PEI hydrogel, the peaks that appeared at 1656  $\text{cm}^{-1}$  and 1710  $\text{cm}^{-1}$  correspond to the  $\text{C}=\text{O}$  stretching vibration for asymmetric  $\text{COO}^-$  and  $-\text{COOH}$ , respectively [48,49]. After the heat treatment, the characteristic peak of the carboxyl group at 1710  $\text{cm}^{-1}$  disappears in the FTIR spectra. The vibration of 1656  $\text{cm}^{-1}$  shifts to a higher wavenumber due to the new bonds forming between the amine and carboxyl groups. This indicates that the carboxylic acid group engaged in the chemical reaction for amide linkage formation [50]. The strong adsorption peak at around 1688  $\text{cm}^{-1}$  is contributed by the  $\text{C}=\text{O}$  stretching vibration in the  $-\text{CONH}-$  bond, which was generated during the thermal crosslinking process. The new absorption peak at 1544  $\text{cm}^{-1}$  is ascribed to the symmetric stretching vibrations of  $-\text{C}(=\text{O})-\text{NH}$  [51,52], which further verify the successful chemical linkage between the carboxyl group and amine group. The peak at 2925  $\text{cm}^{-1}$  is owing to the  $-\text{CH}_2$  symmetric stretching vibration of  $-\text{CH}_2$  [53,54].

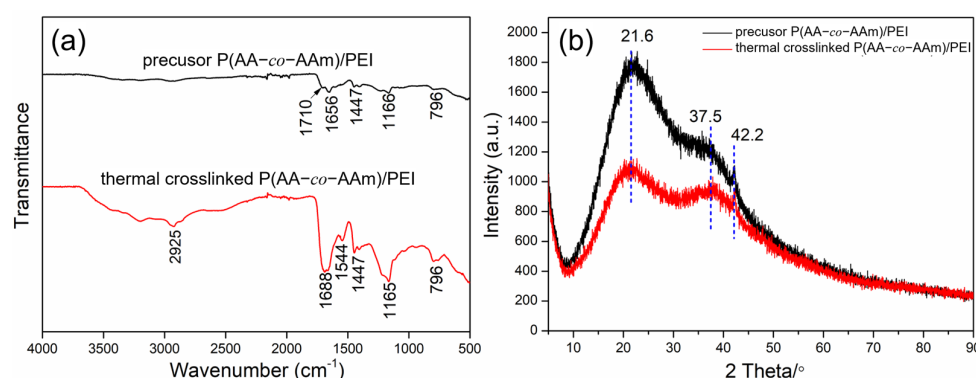


**Figure 3.** FTIR spectra (a) and XRD spectra (b) of precursor hydrogel and thermally crosslinked P(AA-co-AAm)/PEI hydrogel.

The XRD spectrum of precursor P(AA-co-AAm)/PEI hydrogel and thermally crosslinked hydrogel are shown in Figure 3b. The XRD patterns of the two hydrogels do not show obvious crystal order. The peak appeared at  $2\theta = 42.2^\circ$ , attributed to a certain structural regularity of acrylic acid. The broad characteristic peaks at  $2\theta = 21.6^\circ$  and  $37.5^\circ$  reveal the amorphous nature of them. The intensity of thermally crosslinked hydrogel is lower

than that of precursor P(AA-co-AAm)/PEI hydrogel. The reason may be that the thermal crosslinking of PAA and PEI leads to the destruction of the hydrogel crystalline region.

SEM micrographs were obtained to observe the cross-section morphology of the hydrogel samples, and the results are presented in Figure 4. Figure 4a presents the cross-sections of Ti6Al4V substrate covered with coating. The average thickness of the coating is about  $735.6 \pm 18.1 \mu\text{m}$ . The precursor hydrogel and thermally crosslinked P(AA-co-AAm)/PEI hydrogel exhibit a crosslinked network porous structure in Figure 4b. Precursor hydrogel has a loose porous structure in Figure 4(b1). In comparison, the thermally crosslinked P(AA-co-AAm)/PEI hydrogel demonstrates a compact and tight porous structure in Figure 4(b2). The number of porous structures increases concurrently with a decrease in the size of porous structures.

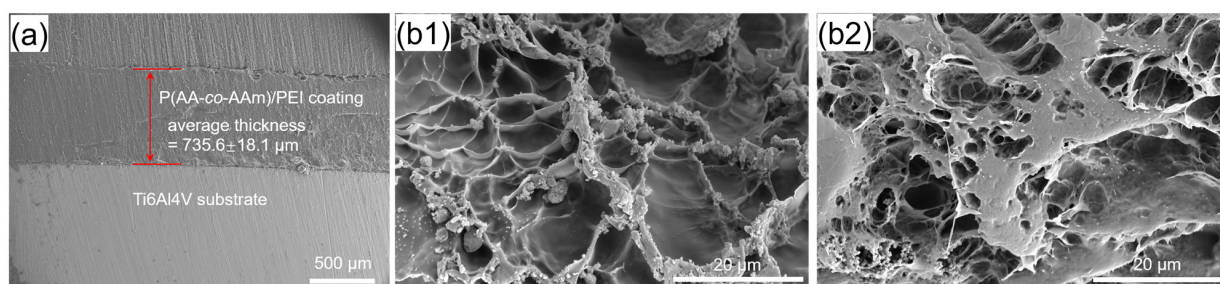


**Figure 4.** Cross-section morphology (a) and microstructure (b) of hydrogel coatings. (b1) precursor hydrogel; (b2) thermally crosslinked P(AA-co-AAm)/PEI hydrogel.

XPS narrow spectra of C1s, O1s, and N1s from the precursor P(AA-co-AAm)/PEI hydrogel and thermally crosslinked hydrogel are displayed in Figure 5. The peaks at different binding energies represent different chemical bonds of elements C, O, and N. High-resolution spectra recorded the curves of the sample with varying contents of PEI. The C1s spectrum of the untreated P(AA-co-AAm)/PEI hydrogel and thermally crosslinked hydrogel can be deconvoluted into three main peaks (Figure 5A), which are assigned to the carbon atoms of C–C (284.5 eV), C–N (285.6 eV), and C=O (288.3 eV), respectively [55,56]. In the O1s spectra (Figure 5B), two fitting peaks are observed at 531.7 and 533.0 eV, corresponding to C=O and C–O, respectively [57]. After heat treatment, there is virtually no binding energy shift in both the C1s and O1s regions. However, a slight decrease in intensity is observed, which may be partially attributed to the declining coverage [58]. Given PEI only contains carbon, nitrogen, and hydrogen without oxygen, the C/O area ratio of the untreated system decreases with increasing PEI content (Figure 5D). After the reaction, the calculated C/O area ratio of the annealed sample is higher than that of the initial sample, indicating oxygen depletion during annealing. The deconvolution of the N1s peak reveals three types of nitrogen bonds in Figure 5C. The binding energy at 399.3 eV corresponds to the C–N. The N1s peak that appeared at 401.2 eV is ascribed to N–H bonds for the P(AA-co-AAm)/PEI hydrogel [59]. Notably, the binding energy of N-containing chemical bonds at 401.2 eV slightly shifts to a higher binding energy after annealing, approximately 401.35 eV, which belongs to the –C(=O)–NH– group [60,61]. That suggests the formation of a chemical reaction between the amine groups and the carboxyl groups by covalent bonding, which is consistent with FITR, XRD, and SEM results.

### 3.3. Surface Wettability

In this research, the quartz plate was covered to the surface of the coating during the preparation process, which eliminates the error in the surface morphology during the contact angle test. Therefore, the surface wettability is primarily controlled by the chemical composition of coatings.

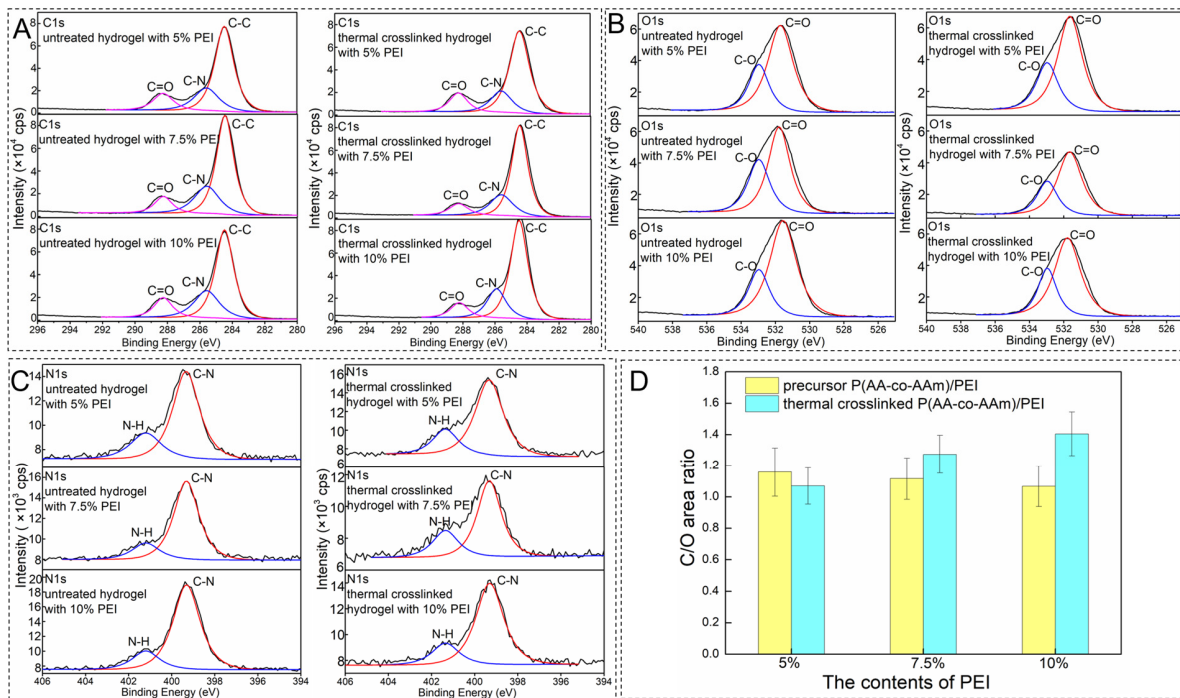


**Figure 5.** XPS spectra of precursor hydrogel and thermally crosslinked P(AA-co-AAm)/PEI hydrogel. (A) C1s; (B) O1s; (C) N1s; (D) C/O area ratio.

Figure 6 illustrates the water contact angle of P(AA-co-AAm)/PEI coatings. The untreated precursor coating exhibits hydrophilicity, with the contact angle remaining 60–71°. This is attributed to the inherent hydrophilic character of coating generated by the abundant carboxyl groups (–COOH) and amine groups (–NH<sub>2</sub>) in molecules. As the content of PEI increases, the contact angle decreases due to the presence of a large number of amine groups in PEI molecules.

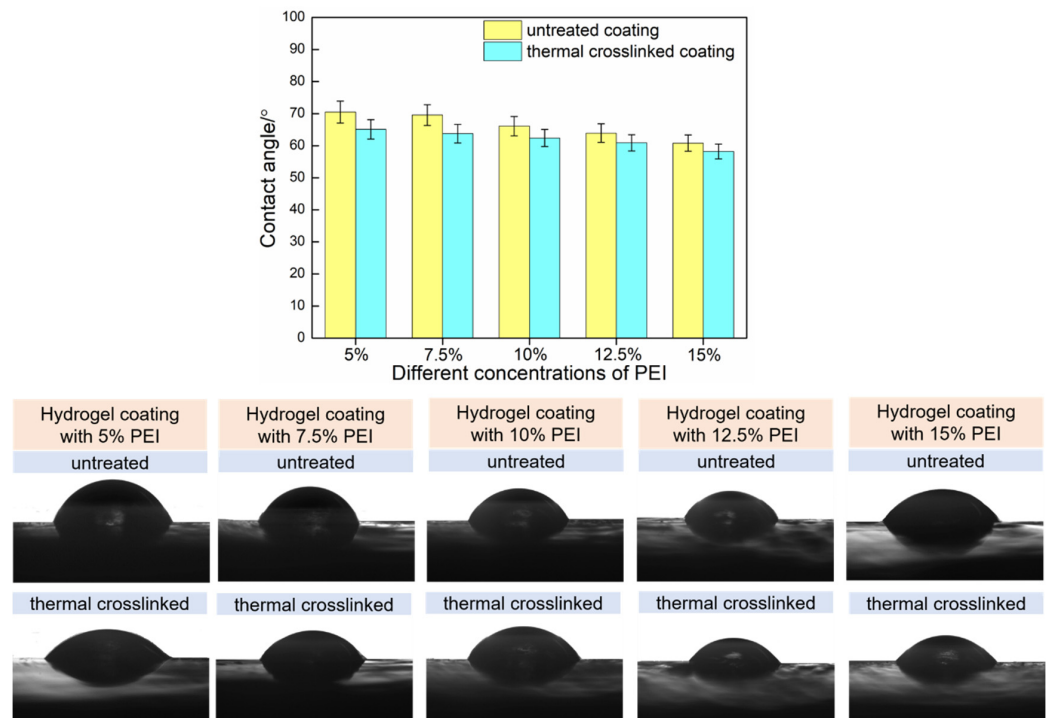


**Figure 6.** The water contact angle of P(AA-co-AAm)/PEI hydrogel coating.

For thermally crosslinked P(AA-co-AAm)/PEI hydrogel coatings,  $-\text{COOH}$  and  $-\text{NH}_2$  groups were transformed into a  $-\text{CO-NH-}$  group, which is the polar and hydrophilicity functional group [62–64]. The abundant presence of polar  $-\text{CO-NH}$  groups notably reduces the contact angle and enhances the hydrophilicity. In Figure 6, the contact angle of the annealed coating is lower than that of the untreated hydrogel coating, about  $2\text{--}5^\circ$  for different PEI contents. The thermally crosslinked hydrogel coating with 15% PEI has the lowest contact angle, approximately  $58.2^\circ$ . It is evident that hydrogel coating produced via thermal crosslinking presents an improvement in the wettability capacity when compared to the untreated coatings.

### 3.4. Porosity and Equilibrium Water Contents

The porosity and equilibrium water content of pristine and thermally crosslinked hydrogel coatings are shown in Figure 7. The influence of PEI concentrations on porosity and equilibrium water content was also evaluated.

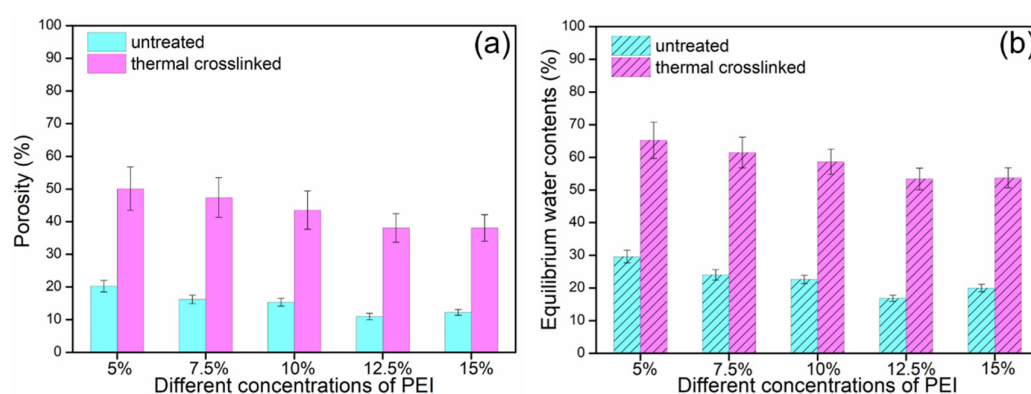


**Figure 7.** Porosity (a) and equilibrium water contents (b) of untreated and thermally crosslinked P(AA-co-AAm)/PEI hydrogel.

As shown in Figure 7a, the thermally crosslinked P(AA-co-AAm)/PEI hydrogel has a higher porosity than that of the untreated coating under identical PEI concentration conditions. At a PEI concentration of 5%, the porosity of untreated coating and thermally crosslinked coating is approximately 20% and 50%, respectively. With the increase in PEI concentration, the porosity gradually decreases. For untreated samples, hydrogel coating with 12.5% PEI has the lowest porosity, about 11%. The porosity of thermally crosslinked hydrogel coating with 12.5% and 15% PEI reaches a stable state, about 38%. The same trend appears in equilibrium water content (Figure 7b). The thermally crosslinked hydrogels present an improvement in the wettability capacity. The equilibrium water contents of hydrogel coating with 5% PEI are 29% for untreated samples and 65% for thermally crosslinked samples, respectively. The equilibrium water content value decreases gradually with the increase in PEI concentration.

The changes in porosity and equilibrium water contents between untreated and thermally crosslinked samples are related to the internal molecular structure of hydrogel coating and its wettability. The heat treatment process generates  $-\text{CO-NH-}$  covalent bonds, which manipulate the internal structure of hydrogel and increase the crosslinking density of PAA, PAAm, and PEI molecules. The increased crosslink density results in elevated porosity [65], thereby affecting the water-holding capacity of hydrogels [66,67]. Owing to its higher porosity (Figure 7a) and wettability (Figure 6), the water molecules are physically trapped by the network structure and more efficiently occupy voids compared to untreated samples due to capillary action [68].

### 3.5. Thermal Properties

The TG-DSC curves of pristine hydrogel and thermally crosslinked hydrogel are shown in Figure 8. At the beginning of the temperature rise, the variation in curves of

pristine hydrogel coating is attributed to the evaporation of physically absorbed water and the dehydration of  $-\text{COOH}$  and  $-\text{NH}_2$  groups. The corresponding total weight loss is 3.68% prior to 150 °C. The thermally crosslinked coating only occurred during the evaporation of physical adsorbed water, with a total weight loss of 3.21% in the TG curve before 150 °C. The pristine hydrogel coating exhibits a higher weight loss than the annealed sample, which confirms the above conclusion. Regarding the DSC curves, both pristine and thermally crosslinked hydrogel coatings have a single endothermic peak at 217.3 °C, respectively, which corresponds to the melting point. At this point, the TG curves display obviously decrease. There is no significant difference in associated weight loss for the samples before and after heat treatment, which is about 11.6% and 10.05%, respectively. TG-DSC results indicate that the hydrogel coating possesses suitable thermal stability.

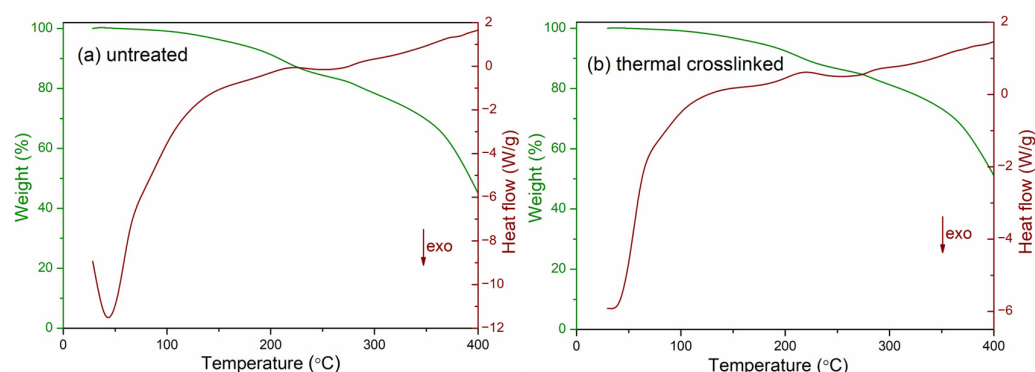


**Figure 8.** DSC and TG curves of untreated (a) and thermally crosslinked (b) P(AA-co-AAm)/PEI hydrogel.

### 3.6. Evaluation of the Lubrication Properties

The lubrication properties of hydrogel coatings were assessed by a ball-on-disk rotating tribometer, and stainless balls were employed as the counterparts. Deionized water, saline, and calf serum were employed as lubrication conditions.

Figure 9a displays the average friction coefficient of thermally crosslinked P(AA-co-AAm)/PEI hydrogel coatings with varying PEI contents. Ti6Al4V substrate and non-thermally crosslinked hydrogel coating serve as the control group. The friction coefficient of the Ti6Al4V substrate is approximately 0.45. Untreated P(AA-co-AAm)/PEI hydrogel coatings with 5% PEI have a slightly lower friction coefficient than the Ti6Al4V substrate, approximately 0.37. With the increase in PEI contents, the friction coefficient increases gradually, even surpassing that of the Ti6Al4V substrate. However, after constructing thermally crosslinked P(AA-co-AAm)/PEI hydrogel coatings on Ti6Al4V substrate, the friction coefficients exhibit a significant reduction compared to the control group. Notably, the friction coefficient of thermally crosslinked P(AA-co-AAm)/PEI hydrogel with 5% PEI is reduced to 0.022. When the PEI content is 5%, 7.5%, 10%, 12.5%, and 15%, the average friction coefficient in deionized water decreases by 93.8%, 91.07%, 85.9%, 83.5%, and 81.7%, respectively, comparing with untreated P(AA-co-AAm)/PEI hydrogel coatings.

The friction test curves of Ti6Al4V substrate, precursor P(AA-co-AAm)/PEI hydrogel coatings, and thermally crosslinked P(AA-co-AAm)/PEI hydrogel coatings are shown in Figure 9b. Compared with Ti6Al4V substrate and untreated P(AA-co-AAm)/PEI hydrogel coatings, thermally crosslinked P(AA-co-AAm)/PEI hydrogel coatings exhibit the lowest friction coefficient. During the testing process, the friction curve remains highly stable, and the friction coefficient is approximately 0.02. The friction curve of the Ti6Al4V substrate displays a slight increase with the increase in sliding time due to the production of abrasive debris. For precursor P(AA-co-AAm)/PEI hydrogel coatings on Ti6Al4V substrate, the friction coefficient increases rapidly and reaches 0.5 within 1 min (Light blue box in Figure 9b and it has been enlarged), which is similar to that of Ti6Al4V substrate. This phenomenon indicates that the precursor P(AA-co-AAm)/PEI hydrogel coatings were worn

out during the initial stage of sliding. The damaged coating hindered the sliding of the two counterparts, resulting in the fluctuation of the friction curve.

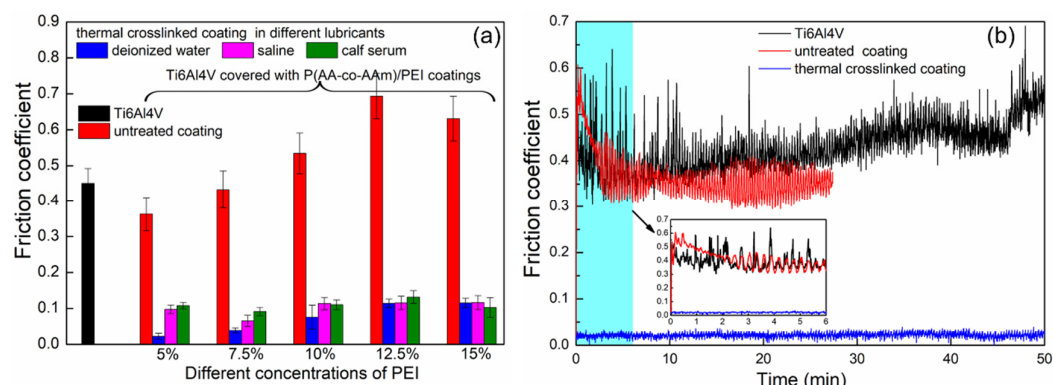


**Figure 9.** Friction coefficient of untreated and thermally crosslinked P(AA-co-AAm)/PEI hydrogel coating. (a) average friction coefficient; (b) variation curve of friction coefficient versus time.

### 3.7. Assessment of the Wear Resistance

Correspondingly, the wear morphology and wear volume of friction pair in distilled water were evaluated by a 3D white light interferometer. The wear morphology of coatings and Ti6Al4V substrate are shown in Figure 10. Each 3D image contains a colorful overall morphology (color) and contour curves (lines and blue shadow). As shown in Figure 10, untreated precursor P(AA-co-AAm)/PEI hydrogel coatings exhibit distinct wear zones and wear volumes. For the precursor hydrogel coating with PEI contents of 5%, 7.5%, and 15%, the maximum depths of wear scar are  $6.8 \pm 0.6 \mu\text{m}$ ,  $14.4 \pm 1.2 \mu\text{m}$ , and  $26.1 \pm 1.7 \mu\text{m}$ , respectively. The width range is from  $1200 \mu\text{m}$  to  $1800 \mu\text{m}$ . The stainless ball exhibits a wear phenomenon, with a wear volume of  $0.32 \pm 0.11 \times 10^6 \mu\text{m}^3$  (Figure 11(b1,b2)). The maximum depth and width of the wear scar on the Ti6Al4V substrate are about  $4.96 \pm 0.4 \mu\text{m}$  and  $852.7 \pm 10.2 \mu\text{m}$  (Figure 10d). There are obviously furrows and scratches, indicating abrasive wear and adhesive wear. This phenomenon also occurs on the surface of the counterpart ball, accompanied by a significant wear volume, about  $8.11 \pm 0.43 \times 10^6 \mu\text{m}^3$  (Figure 11(a1,a2)). After thermal treatment, the hydrogel coating displays a super shallow scratch, which is confirmed by 3D morphology (Figure 10e–g). The depth and width of the wear scar diminish profoundly, and the wear volume of the stainless ball is undetectable (Figure 11(c1,c2)).

The quantitative analyses of the wear volume are shown in Figure 12a. The wear volume of the Ti6Al4V substrate is  $0.38 \pm 0.06 \times 10^6 \mu\text{m}^3$ . It can be seen that the wear volume generated by the deep and wide wear scratch of precursor P(AA-co-AAm)/PEI hydrogel coatings is  $>3 \times 10^6 \mu\text{m}^3$ , which is equal to poor lubricity. Notably, the thermally crosslinked P(AA-co-AAm)/PEI hydrogel coating attained a superior wear volume as low as  $0.028\text{--}0.051 \times 10^6 \mu\text{m}^3$ . That is a significant reduction, even when compared to the Ti6Al4V substrate, with an 86.6%–92.6% reduction. Figure 12b is the SEM wear morphology of the thermally crosslinked P(AA-co-AAm)/PEI coating, showing superficially shallow scratches. The width of the wear scar is approximately  $140.8 \pm 7.1 \mu\text{m}$ , which is significantly lower than that of precursor P(AA-co-AAm)/PEI hydrogel coatings ( $1200\text{--}1800 \mu\text{m}$ , Figure 10a–c) and pristine Ti6Al4V substrate ( $852.7 \mu\text{m}$ , Figure 10d). The wear zone exhibits a slight adhesive wear and furrow. This indicates that the thermally crosslinked P(AA-co-AAm)/PEI hydrogel coating on the surface of Ti6Al4V effectively alleviates the wear behavior during the friction process. The introduction of thermally crosslinked hydrogel enhances the wear resistance and load-bearing capacity during the friction test, indicating that thermally crosslinked P(AA-co-AAm)/PEI hydrogel coatings possess excellent anti-wear properties.

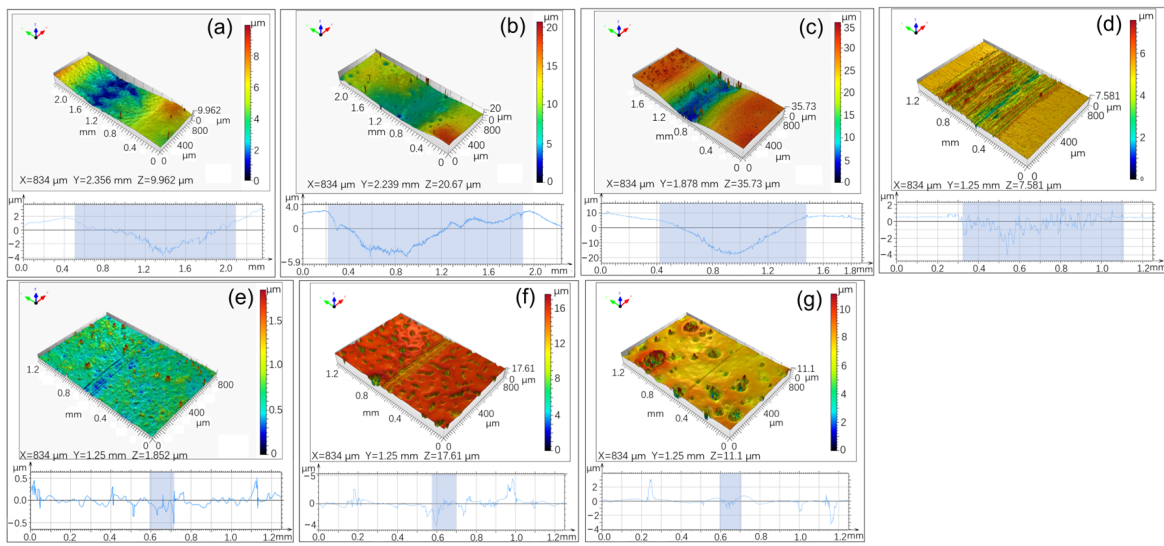


**Figure 10.** The 3D morphologies of wear surfaces and scratch profile after friction test of Ti6Al4V and hydrogel coating. Untreated (a) and thermally crosslinked (e) P(AA-co-AAm)/PEI coatings with 5% PEI. Untreated (b) and thermally crosslinked (f) P(AA-co-AAm)/PEI coatings with 7.5% PEI. Untreated (c) and thermally crosslinked (g) P(AA-co-AAm)/PEI coatings with 15% PEI. Ti6Al4V (d).

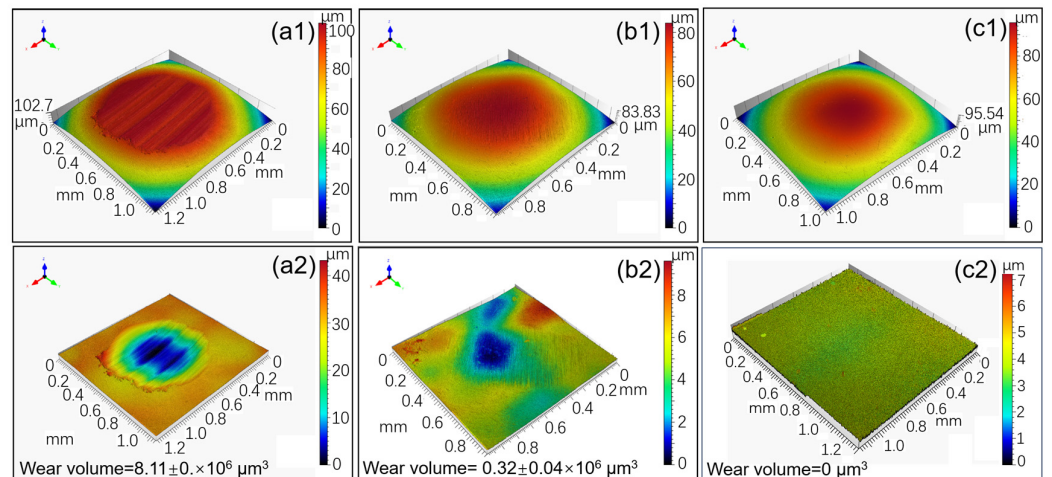


**Figure 11.** Three-dimensional wear morphology and wear volumes of stainless steel ball pair. (a1,a2) Paired with Ti6Al4V. (b1,b2) Paired with untreated P(AA-co-AAm)/PEI coating. (c1,c2) Paired with thermally crosslinked P(AA-co-AAm)/PEI coating.

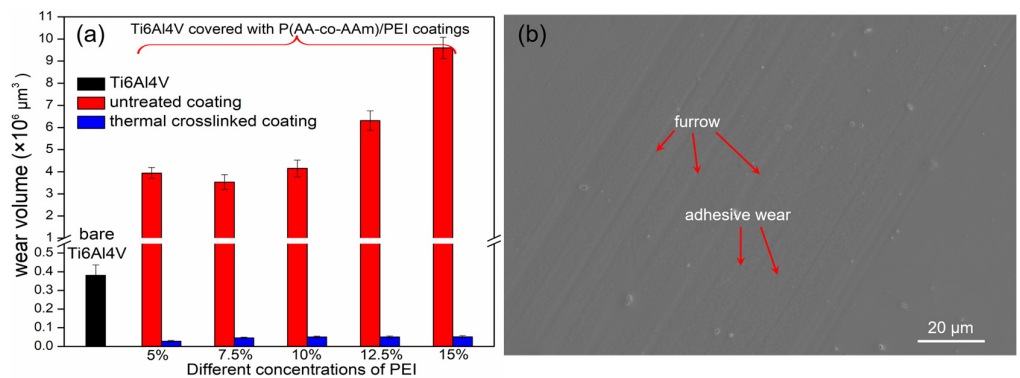


**Figure 12.** Wear volume of hydrogel coating (a) and SEM wear morphology of thermally crosslinked coating (b).

### 3.8. The Lubrication Mechanism of the Composite Hydrogel Coating

According to the experimental results, the thermal treatment P(AA-co-AAm)/PEI hydrogel coatings have excellent lubricating capacity. The preparation of the precursor P(AA-co-AAm)/PEI coating is primarily driven by electrostatic interactions and covalent crosslinking via UV irradiation. Due to the high branch structure of PEI, a large number of amine groups in PEI molecules and carboxyl groups in AA molecules are fully absorbed through electrostatic interactions. The covalent crosslinking arises from the free radical polymerization between AA and AAm molecules. Under the action of the UV initiator,  $-C=C-$  bonds of the monomer molecules break to generate free radicals [69]. During the polymerization process, the crosslinking agent, TEGDMA, promotes the formation of a three-dimensional crosslinking network structure, which is confirmed by Figure 4b.

In the proposed precursor hydrogel coating, the second crosslinked network structure was formed through thermal treatment, as illustrated in Figure 2, achieving covalent bonding between PAA and PEI. The results of FTIR, XRD, and XPS verify the crosslinking reaction. The electrostatic interactions were converted to stable amide covalent bonds from the carboxyl group of PAA and amine groups of PEI, accompanied by the generation of water molecules [70,71]. The chemical reaction includes (i) the dehydrogenation of the  $NH_2$  group in PEI, (ii) the dehydroxylation of the  $COOH$  group in PAA, and (iii) the coupling of the two resulting molecules. Concurrently, during the heating process, the rearrangement of radicals leads to changes in bonding strength and mechanical properties [39].

In the thermally crosslinked hydrogel system, there are two kinds of covalent bonds, the  $-C-C-$  between AA and AAm via UV irradiation and  $-CO-NH-$  between AA and PEI via thermal treatment. That forms two types of crosslinked networks linked by PAA molecules. Due to the addition of  $-CO-NH-$  bonds, the number of covalent bonds and crosslinked networks is higher than that of the precursor hydrogel system. Therefore, the thermally crosslinked P(AA-co-AAm)/PEI hydrogel system is a dual covalent crosslinked network.

During the tribology testing, dual covalent crosslinked networks could effectively resist shear deformation and bear normal loads, compared with precursor hydrogel systems with single crosslinked networks. Furthermore, the  $-CO-NH-$  covalent bonds introduced by thermal treatment result in a stronger bonding force and bonding strength between molecules [39,72]. This enhanced the stability of the coatings and its resistance to shear during the tribological testing, which are ensured by Figures 9–12.

The friction coefficient of thermally crosslinked P(AA-co-AAm)/PEI hydrogel coatings is different in the three lubricants. The friction coefficient remains constant for saline and calf serum lubricant compared with distilled water. This is related to PAA molecules. In this study, the PAA molecules in a crosslinked network participate in the thermal crosslinking reaction. However, due to the limitation of the spatial position of the three-dimensional network structure, a small number of PAA molecules cannot participate in the thermal crosslinking reaction. The intact carboxyl group is retained. In distilled water, negatively charged PAA absorb water to form a hydration sheath, which reduces the self-energy of enclosed charge [73]. This means that it is very difficult to remove water molecules from the hydrated sheath around the charge, which provides suitable hydration lubrication. When the saline was utilized as a lubricant, the net charge of the PAA polyelectrolyte molecules was reduced due to the ion condensation. The addition of salt ions in the aqueous solution shields the electrostatic interaction [74]. The charge screening by salt ions leads to the chain shrinkage of PAA [75]. Electrostatic bridging and polymer chain collapse increase the friction [76]. In calf serum, the negatively charged carboxyl group on the side chains of PAA may attract and adsorb positively charged macromolecules. The existence of protein molecules on both sliding interfaces leads to energy dissipation and increased friction coefficient [77]. With the change in PEI content, the friction coefficient in saline and calf serum is relatively stable compared with that in deionized water. This is related to the content of PAA involved in the thermal crosslinking reaction in the crosslinking network. With the increase in PEI content, more PEI molecules diffuse into the PAA-PAM

three-dimensional network structure, which reduces the constraints of spatial location. As a result, the number of PAA molecules participating in thermal crosslinking increases, leading to a decrease in the number of free carboxyl groups. The number of free carboxyl groups is closely related to the change in friction coefficient in saline and calf serum. The interaction of these reasons makes the friction coefficient slightly higher and relatively stable in saline and calf serum.

At the same time, we compared the experimental results with other similar studies in Table 1. The different types of hydrogel coating were fabricated on the titanium surface via ultraviolet irradiation, freezing–thawing, heat treatment, and other methods. These coatings are applied in the field of biological implants, especially artificial joints. Compared with pure titanium alloys, different degrees of friction coefficient reduction are obtained when hydrogel coating is prepared on titanium. Among them, the hydrogel coating prepared in this study has a low friction coefficient, 0.022.

**Table 1.** The friction coefficient of different hydrogel coating on titanium substrate for bio-implants.

Type of Hydrogel Coating	Titanium Pretreatment	Preparation Method of Hydrogel Coating	Friction Coefficient	References
PVA/HA/PAA	Treated by laser and modified by dopamine	Freeze–thaw and annealing	0.08	[78]
PVA/HA/PAA/PDA	Treated by laser and modified by dopamine	Freeze–thaw and annealing	0.065	[78,79]
PVA-PAM-PMPC	Micro-arc oxidation	UV irradiation and freeze–thaw	0.052	[80]
PVA/PAA/GO/PDA	Modified by 3-aminopropyltriethoxysilane (APTES) and dopamine	Freeze–thaw and annealing	0.144	[81]
PAA-PAM	Polish	UV irradiation	0.085	[19]
double-layer GO and PVP	Treated by laser	Electrophoretic deposition	<0.03	[82]
P(AA-co-AAm)/PEI	Modified by dopamine	UV irradiation and annealing	0.022	this paper

In summary, covalent crosslinking improves the friction and wear stability of the hydrogel coating. The thermally crosslinked P(AA-co-AAm)/PEI hydrogel coatings exhibit efficient lubrication and anti-wear properties. This expands the application of hydrogel materials in the fields of other medical implant materials.

#### 4. Conclusions

In summary, we propose a concise and innovative method for fabricating dual crosslinked hydrogel coating on Ti6Al4V using UV irradiation and heat treatment to improve the tribological properties. The thermally crosslinked P(AA-co-AAm)/PEI hydrogel coatings exhibit better surface wettability and higher porosity than those of untreated hydrogel coatings. The stable low friction coefficient was obtained, approximately 0.022, reducing by 93.8% compared to the pristine Ti6Al4V substrate. The wear volume of the coating was super low, about as low as  $0.028 \times 10^6 \mu\text{m}^3$ , with a 92.6% reduction compared to the Ti6Al4V substrate. No obvious wear scratch could be observed after a period of tribological testing due to excellent wear resistance. The thermally crosslinked P(AA-co-AAm)/PEI hydrogel coating effectively alleviates the wear behavior during the friction process. The newly formed –CO–NH– covalent bonds introduced by thermal treatment have been confirmed as the primary factor for the improvement of lubrication and anti-wear properties. An important requirement for artificial joint applications is stability, low friction, and super low wear. Thus, the thermally crosslinked P(AA-co-AAm)/PEI hydrogel coatings modified Ti6Al4V may find potential applications in artificial joints and other

medical implant materials. Further studies should focus on the relationship between wear resistance and adhesion biocompatibility before clinical applications.

**Author Contributions:** Conceptualization, Y.D.; Methodology, Y.D.; Validation, Y.D.; Formal analysis, Y.X. and Y.H.; Data curation, Y.X. and L.N.; Writing—original draft, Y.D.; Writing—review & editing, Y.X. and L.N.; Supervision, L.N. All authors have read and agreed to the published version of the manuscript.

**Funding:** This work was supported by the Natural Science Foundation of Jiangsu Province (BK20200791), the Nanhu Scholars Program for Young Scholars of XYNU, the High-Level Talents Program of Jinling Institute of Technology (Jit-b-202052), and the open research fund of State Key Laboratory of Organic Electronics and Information Displays (SKL20220001).

**Institutional Review Board Statement:** Not applicable.

**Informed Consent Statement:** Not applicable.

**Data Availability Statement:** Data are contained within the article.

**Conflicts of Interest:** The authors declare that they have no known competing financial interests or personal relationships that could have appeared to influence the work reported in this paper.

## References

1. Cilingir, A.C. Effect of Rotational and Sliding Motions on Friction and Degeneration of Articular Cartilage under Dry and Wet Friction. *J. Bionic Eng.* **2015**, *12*, 464–472. [[CrossRef](#)]
2. Jin, Z.; Dowson, D. Bio-friction. *Friction* **2013**, *1*, 100–113. [[CrossRef](#)]
3. Forster, H.; Fisher, J. The Influence of Loading Time and Lubricant on the Friction of Articular Cartilage. *Proc. Inst. Mech. Eng. Part H J. Eng. Med.* **1996**, *210*, 109–119. [[CrossRef](#)] [[PubMed](#)]
4. Macirowski, T.; Tepic, S.; Mann, R.W. Cartilage Stresses in the Human Hip Joint. *J. Biomech. Eng.* **1994**, *116*, 10–18. [[CrossRef](#)] [[PubMed](#)]
5. Briggs, A.M.; Cross, M.J.; Hoy, D.G.; Sánchez-Riera, L.; Blyth, F.M.; Woolf, A.D.; March, L. Musculoskeletal Health Conditions Represent a Global Threat to Healthy Aging: A Report for the 2015 World Health Organization World Report on Ageing and Health. *Gerontol.* **2016**, *56*, S243–S255. [[CrossRef](#)]
6. Bloyce, A.; Qi, P.Y.; Dong, H.; Bell, T. Surface modification of titanium alloys for combined improvements in corrosion and wear resistance. *Surf. Coat. Technol.* **1998**, *107*, 125–132. [[CrossRef](#)]
7. Pratap, T.; Patra, K. Mechanical micro-texturing of Ti-6Al-4V surfaces for improved wettability and bio-tribological performances. *Surf. Coat. Technol.* **2018**, *349*, 71–81. [[CrossRef](#)]
8. Sawano, H.; Warisawa, S.; Ishihara, S. Study on long life of artificial joints by investigating optimal sliding surface geometry for improvement in wear resistance. *Precis. Eng.* **2009**, *33*, 492–498. [[CrossRef](#)]
9. Luo, Y.; Chen, W.; Tian, M.; Teng, S. Thermal oxidation of Ti6Al4V alloy and its biotribological properties under serum lubrication. *Tribol. Int.* **2015**, *89*, 67–71. [[CrossRef](#)]
10. Chatterji, U.; Ashworth, M.J.; Lewis, P.L.; Dobson, P.J. Effect of total hip arthroplasty on recreational and sporting activity. *ANZ J. Surg.* **2004**, *74*, 446–449. [[CrossRef](#)]
11. Flugsrud, G.B.; Nordsletten, L.; Espehaug, B.; Havelin, L.L.; Meyer, H.E. The effect of middle-age body weight and physical activity on the risk of early revision hip arthroplasty: A cohort study of 1535 individuals. *Acta Orthop.* **2007**, *78*, 99–107. [[CrossRef](#)] [[PubMed](#)]
12. Xu, Y.; Bao, Y.; Liu, Z.; Zheng, Q.; Dong, Y.; Song, R.; Yang, B. Temperature-sensitive tribological performance of titanium alloy lubricated with PNIPAM microgels. *Appl. Surf. Sci.* **2022**, *572*, 151392. [[CrossRef](#)]
13. Mashtalyar, D.V.; Pleshkova, A.I.; Piatkova, M.A.; Nadaraia, K.V.; Imshinetskiy, I.M.; Belov, E.A.; Suchkov, S.N.; Sinebryukhov, S.L.; Gnedenkov, S.V. PTFE-Containing Coating Obtained on Ti by Spraying and PEO Pretreatment. *Coatings* **2023**, *13*, 1249. [[CrossRef](#)]
14. Träger, D.; Słota, D.; Niziołek, K.; Florkiewicz, W.; Sobczak-Kupiec, A. Hybrid Polymer&ndash;Inorganic Coatings Enriched with Carbon Nanotubes on Ti-6Al-4V Alloy for Biomedical Applications. *Coatings* **2023**, *13*, 1813.
15. Zhao, Y.; Chen, X.; Li, S.; Zeng, R.; Zhang, F.; Wang, Z.; Guan, S. Corrosion resistance and drug release profile of gentamicin-loaded polyelectrolyte multilayers on magnesium alloys: Effects of heat treatment. *J. Colloid Interface Sci.* **2019**, *547*, 309–317. [[CrossRef](#)] [[PubMed](#)]
16. Liu, X.; Li, Y.; Li, S.; Lin, Y.-C.; Li, V.L.; Chen, Y.-H.; Lin, C.; Keerthi, M.; Shih, S.-J.; Chung, R.-J. Polyelectrolyte multilayer coatings for short/long-term release of antibacterial agents. *Surf. Coat. Technol.* **2020**, *393*, 125696. [[CrossRef](#)]
17. Zhou, X.; Wang, Z.; Li, T.; Liu, Z.; Sun, X.; Wang, W.; Chen, L.; He, C. Enhanced tissue infiltration and bone regeneration through spatiotemporal delivery of bioactive factors from polyelectrolytes modified biomimetic scaffold. *Mater. Today Bio* **2023**, *20*, 100681. [[CrossRef](#)]

18. Deng, Y.; Xu, Y.; Ni, X.; Li Yu, W.; Wang, Y.; Yang, Z. Mechanical and Tribological Behavior of Branched Polyethyleneimine/Polyacrylic Acid Coatings on Ti6Al4V Substrate. *J. Mater. Eng. Perform.* **2023**, *32*, 6123–6132. [[CrossRef](#)]
19. Deng, Y.; Sun, J.; Ni, X.; Yu, B. Tribological properties of hierarchical structure artificial joints with poly acrylic acid (AA)—Poly acrylamide (AAm) hydrogel and Ti6Al4V substrate. *J. Polym. Res.* **2020**, *27*, 157. [[CrossRef](#)]
20. Deng, Y.; Xiong, D. Fabrication and properties of UHMWPE grafted with acrylamide polymer brushes. *J. Polym. Res.* **2015**, *22*, 195. [[CrossRef](#)]
21. Xiong, D.; Deng, Y.; Wang, N.; Yang, Y. Influence of surface PMPC brushes on tribological and biocompatibility properties of UHMWPE. *Appl. Surf. Sci.* **2014**, *298*, 56–61. [[CrossRef](#)]
22. Hafezi, M.; Qin, L.; Mahmoodi, P.; Yang, H.; Dong, G. Releasable agarose-hyaluronan hydrogel with anti-friction performance and enhanced stability for artificial joint applications. *Tribol. Int.* **2021**, *153*, 106622. [[CrossRef](#)]
23. Feng, S.; Liu, Y.; Li, J.; Wen, S. Superlubricity Achieved with Zwitterionic Brushes in Diverse Conditions Induced by Shear Actions. *Macromolecules* **2021**, *54*, 5719–5727. [[CrossRef](#)]
24. Vilela, C.A.; Correia, C.; da Silva Morais, A.; Santos, T.C.; Gertrudes, A.C.; Moreira, E.S.; Frias, A.M.; Learmonth, D.A.; Oliveira, P.; Oliveira, J.M.; et al. In vitro and in vivo performance of methacrylated gellan gum hydrogel formulations for cartilage repair\*. *J. Biomed. Mater. Res. Part A* **2018**, *106*, 1987–1996. [[CrossRef](#)] [[PubMed](#)]
25. Hua, Y.; Xia, H.; Jia, L.; Zhao, J.; Zhao, D.; Yan, X.; Zhang, Y.; Tang, S.; Zhou, G.; Zhu, L.; et al. Ultrafast, tough, and adhesive hydrogel based on hybrid photocrosslinking for articular cartilage repair in water-filled arthroscopy. *Sci. Adv.* **2021**, *7*, eabg0628. [[CrossRef](#)] [[PubMed](#)]
26. Yang, F.; Zhao, J.; Koshut, W.J.; Watt, J.; Riboh, J.C.; Gall, K.; Wiley, B.J. A Synthetic Hydrogel Composite with the Mechanical Behavior and Durability of Cartilage. *Adv. Funct. Mater.* **2020**, *30*, 2003451. [[CrossRef](#)]
27. Wei, Q.; Liu, H.; Zhao, X.; Zhao, W.; Xu, R.; Ma, S.; Zhou, F. Bio-inspired hydrogel-polymer brush bi-layered coating dramatically boosting the lubrication and wear-resistance. *Tribol. Int.* **2023**, *177*, 108000. [[CrossRef](#)]
28. Gong, J.P.; Katsuyama, Y.; Kurokawa, T.; Osada, Y. Double-Network Hydrogels with Extremely High Mechanical Strength. *Adv. Mater.* **2003**, *15*, 1155–1158. [[CrossRef](#)]
29. Pathak, A.K.; Singh, V.K. A wide range and highly sensitive optical fiber pH sensor using polyacrylamide hydrogel. *Opt. Fiber Technol.* **2017**, *39*, 43–48. [[CrossRef](#)]
30. Jing, Z.; Xu, A.; Liang, Y.-Q.; Zhang, Z.; Yu, C.; Hong, P.; Li, Y. Biodegradable Poly(acrylic acid-co-acrylamide)/Poly(vinyl alcohol) Double Network Hydrogels with Tunable Mechanics and High Self-healing Performance. *Polymers* **2019**, *11*, 952. [[CrossRef](#)]
31. Muniz, E.C.; Geuskens, G. Compressive Elastic Modulus of Polyacrylamide Hydrogels and Semi-IPNs with Poly(N-isopropylacrylamide). *Macromolecules* **2001**, *34*, 4480–4484. [[CrossRef](#)]
32. Means, A.K.; Shrode, C.S.; Whitney, L.V.; Ehrhardt, D.A.; Grunlan, M.A. Double Network Hydrogels that Mimic the Modulus, Strength, and Lubricity of Cartilage. *Biomacromolecules* **2019**, *20*, 2034–2042. [[CrossRef](#)] [[PubMed](#)]
33. Shahzamani, M.; Taheri, S.; Roghanizad, A.; Naseri, N.; Dinari, M. Preparation and characterization of hydrogel nanocomposite based on nanocellulose and acrylic acid in the presence of urea. *Int. J. Biol. Macromol.* **2020**, *147*, 187–193. [[CrossRef](#)] [[PubMed](#)]
34. Cozens, E.J.; Roohpour, N.; Gautrot, J.E. Comparative adhesion of chemically and physically crosslinked poly(acrylic acid)-based hydrogels to soft tissues. *Eur. Polym. J.* **2021**, *146*, 110250. [[CrossRef](#)]
35. Erceg, T.; Cakić, S.; Cvetinov, M.; Dapčević-Hadnađev, T.; Budinski-Simendić, J.; Ristić, I. The properties of conventionally and microwave synthesized poly(acrylamide-co-acrylic acid) hydrogels. *Polym. Bull.* **2020**, *77*, 2089–2110. [[CrossRef](#)]
36. Kim, D.; Park, K. Swelling and mechanical properties of superporous hydrogels of poly(acrylamide-co-acrylic acid)/polyethylenimine interpenetrating polymer networks. *Polymer* **2004**, *45*, 189–196. [[CrossRef](#)]
37. Caruso, F.; Lichtenfeld, H.; Donath, E.; Möhwald, H. Investigation of Electrostatic Interactions in Polyelectrolyte Multilayer Films: Binding of Anionic Fluorescent Probes to Layers Assembled onto Colloids. *Macromolecules* **1999**, *32*, 2317–2328. [[CrossRef](#)]
38. Zhu, X.; Jańczewski, D.; Lee, S.S.C.; Teo, S.L.-M.; Vancso, G.J. Cross-Linked Polyelectrolyte Multilayers for Marine Antifouling Applications. *ACS Appl. Mater. Interfaces* **2013**, *5*, 5961–5968. [[CrossRef](#)]
39. Zhang, S.-w.; Feng, D.; Wang, D. Tribological behaviors of composite molecular deposition films. *Tribol. Int.* **2005**, *38*, 959–965. [[CrossRef](#)]
40. Král, M.; Dendisová, M.; Matějka, P.; Svoboda, J.; Pop-Georgievski, O. Infrared imaging of surface confluent polydopamine (PDA) films at the nanoscale. *Colloids Surf. B Biointerfaces* **2023**, *221*, 112954. [[CrossRef](#)]
41. Mondal, A.; Devine, R.; Estes, L.; Manuel, J.; Singha, P.; Mancha, J.; Palmer, M.; Handa, H. Highly hydrophobic polytetrafluoroethylene particle immobilization via polydopamine anchor layer on nitric oxide releasing polymer for biomedical applications. *J. Colloid Interface Sci.* **2021**, *585*, 716–728. [[CrossRef](#)] [[PubMed](#)]
42. Tran, V.T.; Mredha, M.T.I.; Jeon, I. High-water-content hydrogels exhibiting superior stiffness, strength, and toughness. *Extrem. Mech. Lett.* **2020**, *37*, 100691. [[CrossRef](#)]
43. Santos, L.; Ferraz, M.P.; Shirosaki, Y.; Lopes, M.A.; Fernandes, M.H.; Osaka, A.; Santos, J.D. Degradation Studies and Biological Behavior on an Artificial Cornea Material. *Investig. Ophthalmol. Vis. Sci.* **2011**, *52*, 4274–4281. [[CrossRef](#)] [[PubMed](#)]
44. Cao, D.; Zhang, Y.; Cui, Z.; Du, Y.; Shi, Z. New strategy for design and fabrication of polymer hydrogel with tunable porosity as artificial corneal skirt. *Mater. Sci. Eng. C* **2017**, *70*, 665–672. [[CrossRef](#)] [[PubMed](#)]
45. Zhou, Y.; Xu, N.; Tian, K.; Qing, T.; Hao, Y.; Liang, P.; Li, M. Nitritotriacetic acid modified magnetic Prussian blue for efficient removal of cadmium from wastewater. *Appl. Surf. Sci.* **2022**, *600*, 154102. [[CrossRef](#)]

46. Ji, J.; Ke, Y.; Pei, Y.; Zhang, G. Effects of highly exfoliated montmorillonite layers on the properties of clay reinforced terpolymer nanocomposite plugging microspheres. *J. Appl. Polym. Sci.* **2017**, *134*, 44894. [[CrossRef](#)]
47. Li, K.; Zhang, C.; Du, Z.; Li, H.; Zou, W. Preparation of humidity-responsive antistatic carbon nanotube/PEI nanocomposites. *Synth. Met.* **2012**, *162*, 2010–2015. [[CrossRef](#)]
48. Liu, Y.; Fu, R.; Sun, Y.; Zhou, X.; Baig, S.A.; Xu, X. Multifunctional nanocomposites Fe<sub>3</sub>O<sub>4</sub>@SiO<sub>2</sub>-EDTA for Pb(II) and Cu(II) removal from aqueous solutions. *Appl. Surf. Sci.* **2016**, *369*, 267–276. [[CrossRef](#)]
49. Sehaqui, H.; de Larraya, U.P.; Liu, P.; Pfenninger, N.; Mathew, A.P.; Zimmermann, T.; Tingaut, P. Enhancing adsorption of heavy metal ions onto biobased nanofibers from waste pulp residues for application in wastewater treatment. *Cellulose* **2014**, *21*, 2831–2844. [[CrossRef](#)]
50. Lee, H.; Sun, J.-Y. Strong and Facile Adhesives Based on Phase Transitional Poly(acrylic acid)/Poly(ethylenimine) Complexes. *ACS Appl. Eng. Mater.* **2023**, *1*, 229–240. [[CrossRef](#)]
51. Tang, S.; Lin, L.; Wang, X.; Sun, X.; Yu, A. Adsorption of fulvic acid onto polyamide 6 microplastics: Influencing factors, kinetics modeling, site energy distribution and interaction mechanisms. *Chemosphere* **2021**, *272*, 129638. [[CrossRef](#)] [[PubMed](#)]
52. He, J.; Jiang, Z.; Fu, X.; Ni, F.; Shen, F.; Zhang, S.; Cheng, Z.; Lei, Y.; Zhang, Y.; He, Y. Unveiling interactions of norfloxacin with microplastic in surface water by 2D FTIR correlation spectroscopy and X-ray photoelectron spectroscopy analyses. *Ecotoxicol. Environ. Saf.* **2023**, *251*, 114521. [[CrossRef](#)] [[PubMed](#)]
53. Xie, X.; Zhang, L.; Luo, X.; Su, T.; Zhang, Y.; Qin, Z.; Ji, H. PEI modified magnetic porous cassava residue microspheres for adsorbing Cd(II) from aqueous solution. *Eur. Polym. J.* **2021**, *159*, 110741. [[CrossRef](#)]
54. Yu, D.; Wang, Y.; Wu, M.; Zhang, L.; Wang, L.; Ni, H. Surface functionalization of cellulose with hyperbranched polyamide for efficient adsorption of organic dyes and heavy metals. *J. Clean. Prod.* **2019**, *232*, 774–783. [[CrossRef](#)]
55. Wang, Y.; Chen, G.; Weng, H.; Wang, L.; Chen, J.; Cheng, S.; Zhang, P.; Wang, M.; Ge, X.; Chen, H.; et al. Carbon-doped boron nitride nanosheets with adjustable band structure for efficient photocatalytic U(VI) reduction under visible light. *Chem. Eng. J.* **2021**, *410*, 128280. [[CrossRef](#)]
56. Zhang, T.; Xu, Y.; Li, H.; Zhang, B. Interfacial adhesion between carbon fibers and nylon 6: Effect of fiber surface chemistry and grafting of nano-SiO<sub>2</sub>. *Compos. Part A Appl. Sci. Manuf.* **2019**, *121*, 157–168. [[CrossRef](#)]
57. Li, L.; Huang, S.; Wen, T.; Ma, R.; Yin, L.; Li, J.; Chen, Z.; Hayat, T.; Hu, B.; Wang, X. Fabrication of carboxyl and amino functionalized carbonaceous microspheres and their enhanced adsorption behaviors of U(VI). *J. Colloid Interface Sci.* **2019**, *543*, 225–236. [[CrossRef](#)]
58. Yang, B.; Niu, K.; Haag, F.; Cao, N.; Zhang, J.; Zhang, H.; Li, Q.; Allegretti, F.; Björk, J.; Barth, J.V.; et al. Abiotic Formation of an Amide Bond via Surface-Supported Direct Carboxyl–Amine Coupling. *Angew. Chem. Int. Ed.* **2022**, *61*, e202113590. [[CrossRef](#)]
59. Wang, Y.; Gu, Z.; Yang, J.; Liao, J.; Yang, Y.; Liu, N.; Tang, J. Amidoxime-grafted multiwalled carbon nanotubes by plasma techniques for efficient removal of uranium(VI). *Appl. Surf. Sci.* **2014**, *320*, 10–20. [[CrossRef](#)]
60. Ma, L.; Wu, G.; Zhao, M.; Li, X.; Han, P.; Song, G. Modification of carbon fibers surfaces with polyetheramines: The role of interphase microstructure on adhesion properties of CF/epoxy composites. *Polym. Compos.* **2018**, *39*, E2346–E2355. [[CrossRef](#)]
61. Pan, M.; Cruz, G.M.; Gazon, C.; Kechkeche, D.; Renault, L.H.; Clavier, G.; Méallet-Renault, R. Luminescence-Sensitive Surfaces Bearing Ratiometric Nanoparticles for Bacteria Growth Detection. *ACS Appl. Polym. Mater.* **2022**, *4*, 5482–5492. [[CrossRef](#)]
62. Zhai, S.; Li, M.; Wang, D.; Ju, X.; Fu, S. Cyano and acylamino group modification for tannery sludge bio-char: Enhancement of adsorption universality for dye pollutants. *J. Environ. Chem. Eng.* **2021**, *9*, 104939. [[CrossRef](#)]
63. Wang, Z.; Dong, Y.; Yang, J.-C.; Wang, X.-J.; Zhang, M.-l.; Zhang, G.; Long, S.-R.; Liu, S.; Yang, J. Improved interfacial shear strength in carbon fiber enhanced semi-aromatic polyamide 6T composite via in-situ polymerization on fiber surface. *Compos. Sci. Technol.* **2022**, *223*, 109401. [[CrossRef](#)]
64. Wu, Y.; Han, C.; Yang, J.; Jia, S.; Wang, S. Polypropylene films modified by air plasma and feather keratin graft. *Surf. Coat. Technol.* **2011**, *206*, 506–510. [[CrossRef](#)]
65. Sun, D.; Wang, J.; Wang, H.; Yan, Z.; Ma, W.; Ma, X.; Wang, Y.; Ma, Z.; Jin, X.; Sun, S.; et al. Influence of crosslink density on the interfacial bonding performance for epoxy resin towards load-induced calcium silicate hydrate gel. *J. Non-Cryst. Solids* **2023**, *619*, 122553. [[CrossRef](#)]
66. Souza Almeida, F.; Guedes Silva, K.C.; Matias Navarrete de Toledo, A.; Kawazoe Sato, A.C. Modulating porosity and mechanical properties of pectin hydrogels by starch addition. *J. Food Sci. Technol.* **2021**, *58*, 302–310. [[CrossRef](#)] [[PubMed](#)]
67. Mohammadian, M.; Madadlou, A. Cold-set hydrogels made of whey protein nanofibrils with different divalent cations. *Int. J. Biol. Macromol.* **2016**, *89*, 499–506. [[CrossRef](#)]
68. Almeida, A.P.C.; Saraiva, J.N.; Cavaco, G.; Portela, R.P.; Leal, C.R.; Sobral, R.G.; Almeida, P.L. Crosslinked bacterial cellulose hydrogels for biomedical applications. *Eur. Polym. J.* **2022**, *177*, 111438. [[CrossRef](#)]
69. Deng, Y.; Xiong, D.; Wang, K. The mechanical properties of the ultra high molecular weight polyethylene grafted with 3-dimethyl (3-(N-methacryamido) propyl) ammonium propane sulfonate. *J. Mech. Behav. Biomed. Mater.* **2014**, *35*, 18–26. [[CrossRef](#)]
70. Huang, X.; Chrisman, J.D.; Zacharia, N.S. Omniphobic Slippery Coatings Based on Lubricant-Infused Porous Polyelectrolyte Multilayers. *ACS Macro Lett.* **2013**, *2*, 826–829. [[CrossRef](#)]
71. Gu, Y.; Huang, X.; Wiener, C.G.; Vogt, B.D.; Zacharia, N.S. Large-Scale Solvent Driven Actuation of Polyelectrolyte Multilayers Based on Modulation of Dynamic Secondary Interactions. *ACS Appl. Mater. Interfaces* **2015**, *7*, 1848–1858. [[CrossRef](#)] [[PubMed](#)]

72. Cao, X.; Pettitt, M.E.; Wode, F.; Arpa Sancet, M.P.; Fu, J.; Ji, J.; Callow, M.E.; Callow, J.A.; Rosenhahn, A.; Grunze, M. Interaction of Zoospores of the Green Alga *Ulva* with Bioinspired Micro- and Nanostructured Surfaces Prepared by Polyelectrolyte Layer-by-Layer Self-Assembly. *Adv. Funct. Mater.* **2010**, *20*, 1984–1993. [[CrossRef](#)]
73. Klein, J. Hydration lubrication. *Friction* **2013**, *1*, 1–23. [[CrossRef](#)]
74. Sappidi, P.; Natarajan, U. Effect of salt valency and concentration on structure and thermodynamic behavior of anionic polyelectrolyte Na<sup>+</sup>-polyethacrylate aqueous solution. *J. Mol. Model.* **2016**, *22*, 274. [[CrossRef](#)] [[PubMed](#)]
75. Schweins, R.; Hollmann, J.; Huber, K. Dilute solution behaviour of sodium polyacrylate chains in aqueous NaCl solutions. *Polymer* **2003**, *44*, 7131–7141. [[CrossRef](#)]
76. Yu, J.; Jackson, N.E.; Xu, X.; Brettmann, B.K.; Ruths, M.; de Pablo, J.J.; Tirrell, M. Multivalent ions induce lateral structural inhomogeneities in polyelectrolyte brushes. *Sci. Adv.* **2017**, *3*, eaao1497. [[CrossRef](#)]
77. Xu, J.; Zhang, C.; Luo, J. Hydration Lubrication Applicable to Artificial Joints through Polyelectrolyte-Embedded Modification on UHMWPE. *ACS Appl. Polym. Mater.* **2022**, *4*, 7487–7497. [[CrossRef](#)]
78. Chen, K.; Liu, S.; Wu, X.; Wang, F.; Chen, G.; Yang, X.; Xu, L.; Qi, J.; Luo, Y.; Zhang, D. Mussel-inspired construction of Ti6Al4V-hydrogel artificial cartilage material with high strength and low friction. *Mater. Lett.* **2020**, *265*, 127421. [[CrossRef](#)]
79. Chen, Q.; Zhang, X.; Liu, S.; Chen, K.; Feng, C.; Li, X.; Qi, J.; Luo, Y.; Liu, H.; Zhang, D. Cartilage-bone inspired the construction of soft-hard composite material with excellent interfacial binding performance and low friction for artificial joints. *Friction* **2023**, *11*, 1177–1193. [[CrossRef](#)]
80. Cui, L.; Li, H.; Huang, J.; Xiong, D. Improved biotribological performance of Ti6Al4V alloy through the synergetic effects of porous TiO<sub>2</sub> layer and zwitterionic hydrogel coating. *Ceram. Int.* **2021**, *47*, 34970–34978. [[CrossRef](#)]
81. Wang, C.; Zhu, K.; Gao, Y.; Han, S.; Ju, J.; Ren, T.; Zhao, X. Multifunctional GO-based hydrogel coating on Ti-6Al-4 V Alloy with enhanced bioactivity, anticorrosion and tribological properties against cortical bone. *Tribol. Int.* **2023**, *184*, 108423. [[CrossRef](#)]
82. Sadeghi, M.; Kharaziha, M.; Salimijazi, H.R. Double layer graphene oxide-PVP coatings on the textured Ti6Al4V for improvement of frictional and biological behavior. *Surf. Coat. Technol.* **2019**, *374*, 656–665. [[CrossRef](#)]

**Disclaimer/Publisher’s Note:** The statements, opinions and data contained in all publications are solely those of the individual author(s) and contributor(s) and not of MDPI and/or the editor(s). MDPI and/or the editor(s) disclaim responsibility for any injury to people or property resulting from any ideas, methods, instructions or products referred to in the content.